Journal of Solid State Chemistry **166,** 341–351 (2002)
doi:10.1006/jssc.2002.9602

Hydrothermal Synthesis of Lithium Zinc Phosphates: Structural Investigation of Twinned α-$Li_4Zn(PO_4)_2$ and a High Temperature Polymorph β-$Li_4Zn(PO_4)_2$

T. R. Jensen,*[,1] R. G. Hazell,* A. Nørlund Christensen,* and J. C. Hanson†

*Department of Chemistry, University of Aarhus, DK-8000 Århus C, Denmark; and †Chemistry Department, Brookhaven National Laboratory, Upton, New York 11973

Received November 15, 2001; in revised form March 25, 2002; accepted April 3, 2002

The system LiOH:$Zn(NO_3)_2$:H_3PO_4:H_2O was investigated using hydrothermal synthesis techniques in the temperature range $20°C < T < 602°C$ and pressure range, $1 < p < 2.8$ kbar, and the crystallization fields of some lithium zinc orthophosphates are reported. Small crystals of a twinned lithium zinc phosphate, α-$Li_4Zn(PO_4)_2$ were prepared and a structural investigation was performed using synchrotron X-ray diffraction: monoclinic, space group $P2_1/a$, $a = 8.096(2)$ Å, $b = 10.242(2)$ Å, $c = 8.106(2)$ Å, $\beta = 104.73(3)°$, $V = 650.1(2)$ Å^3 and $Z = 4$. The refinement gave $R(F) = 0.042$ and $wR(F^2) = 0.068$ based on 968 independent reflections and 616 observed, $F_o^2 > 3\sigma(F_o^2)$ ($\lambda = 0.9346(1)$ Å). The cations are tetrahedrally coordinated to oxygen, and the structure can be viewed as layers of regular ZnO_4 and PO_4 tetrahedra interconnected by more distorted LiO_4 tetrahedra. Thermal investigation using in situ powder X-ray diffraction in the temperature range $20°C < T < 900°C$ was performed. The reversible phase transition α → β-$Li_4Zn(PO_4)_2$ was observed in agreement with previous investigations. A powder pattern measured at $T = 900°C$ was indexed with a triclinic unit cell: space group $P\bar{1}$, $a = 5.173(3)$ Å, $b = 7.97(1)$ Å, $c = 9.92(1)$ Å, $\alpha = 80.9(1)°$, $\beta = 126.8(1)°$ and $\gamma = 106.0(1)°$, $V = 319.8(7)$ Å^3 and $Z = 2$. The linear thermal expansion of α- and β-$Li_4Zn(PO_4)_2$ are extracted from powder diffraction data in the temperature range RT to 900°C. © 2002 Elsevier Science (USA)

Key Words: **lithium zinc phosphate; hydrothermal synthesis; crystal structure; synchrotron radiation; thermal investigation; in situ powder diffraction.**

1. INTRODUCTION

The phosphate chemistry has received considerable interest during the past decades and has provided a variety of new materials revealing a great structural diversity ranging from mesoporous to more dense phases (1–5). Introduction of monovalent ions, e.g., lithium, in phosphate materials can be of interest for ion conduction properties such as rechargeable lithium batteries (6).

Hydrothermal preparation techniques have revealed existence of several new lithium zinc phosphates and two hydrated zeolite-like polymorphs of $LiZnPO_4 \cdot H_2O$ were also described (3, 7, 8). One polymorph is isomorphous with zeolite ABW (space group $Pna2_1$) (3, 7), denoted α-$LiZnPO_4 \cdot H_2O$. β-$LiZnPO_4 \cdot H_2O$ (space group $P2_1ab$) is a new variant of the ABW topology having the ABW connectivity of tetrahedra but the tetrahedra in the four ring zig–zag chains are pointing alternatingly up (U) and down (D) with the sequence UUDD, whereas in α-$LiZnPO_4 \cdot H_2O$ all tetrahedra point in the same direction, viewed along the *c*-axis (8). At temperatures higher than ca. 100°C more dense materials can be prepared, e.g., a phenacite-like compound ε-$LiZnPO_4$ (9) (denoted ε-$LiZnPO_4$ in this work for distinction from other polymorphs) and a cristobalite-related phase, δ_I-$LiZnPO_4$ (7, 10). Furthermore, two complex phases have been described, α-$LiZnPO_4$ (11–13) and CR1-$LiZnPO_4$ (14). The lithium zinc phosphates show a larger variety of phases than the corresponding arsenates where only two phases are known. A phenacite-like material, α-$LiZnAsO_4$, can be obtained by solid-state reaction (15) and by hydrothermal synthesis (16) along with a phase isomorphous to zeolite ABW, $LiZnAsO_4 \cdot H_2O$ (3, 17). A large number of new members in the system, M_2O–ZnO–P_2O_5–H_2O, M = alkali metal, were discovered during the last decade, partly due to development of low-temperature hydrothermal synthesis methods (see e.g., Refs. (3, 18–21)). Solid-state synthesis and thermal analysis have provided insight in the phase diagram for the system Li_3PO_4–$Zn_3(PO_4)_2$ and knowledge of a variety of relatively dense phases. The equilibrium phase diagram shows existence of four lithium zinc

[1] To whom correspondence should be addressed. Fax: +45-8619-6199. E-mail: trj@chem.au.dk.

0022-4596/02 $35.00

phosphates, $Li_4Zn(PO_4)_2$, $Li_9Zn_6(PO_4)_7$, $LiZnPO_4$, $LiZn_9(PO_4)_7$, and each of them may exist in one, two or three modifications (22). The phase α-$Li_4Zn(PO_4)_2$ was discovered by Belov *et al.* (23), and a reversible phase transition, $\alpha \leftrightarrow \beta$, at $T = 425°C$ was described by Torres-Trevino and West (22, 24). The high-temperature polymorph β could be quenched to RT by substitution of ca. 10% of the phosphorous by silicon. A powder pattern was measured at RT and indexed with an orthorhombic unit cell (22).

In a search for new materials, we explored the system $LiOH:Zn(NO_3)_2:H_3PO_4:H_2O$, the crystallization fields of the compounds are reported. A method for hydrothermal synthesis of α-$Li_4Zn(PO_4)_2$ is presented together with the detailed crystal structure of twinned α-$Li_4Zn(PO_4)_2$. The reversible phase transition to the high-temperature polymorph, β-$Li_4Zn(PO_4)_2$ is studied by in situ powder diffraction, also providing information on the thermal expansion of α- and β-$Li_4Zn(PO_4)_2$.

2. EXPERIMENTAL

2.1. Hydrothermal Synthesis

The crystallization fields of lithium zinc phosphates formed in the system, $LiOH:Zn(NO_3)_2:H_3PO_4:H_2O$ were investigated using systematic hydrothermal synthesis. A number of experiments were carried out using different amounts of $LiOH \cdot H_2O$ and different temperatures in the range 20–240°C in order to give a more detailed description of the phase stability fields of the compounds formed in the system, $LiOH:Zn(NO_3)_2:H_3PO_4:H_2O$. Two series of syntheses were performed using phosphate concentrations of $C(PO_4^{3-}) \approx 0.30$ M (**A**) and $C(PO_4^{3-}) \approx 0.48$ M (**B**). A clear solution, **A**, was prepared by dissolving H_3PO_4 (10.726 g) and $Zn(NO_3)_2 \cdot 6H_2O$ (27.642 g) in H_2O and diluting to 100 mL. A solution, **B**, was prepared in a similar way using H_3PO_4 (16.518 g) and $Zn(NO_3)_2 \cdot 6H_2O$ (42.563 g). The syntheses were performed by dissolving different amounts of $LiOH \cdot H_2O$ in 10 mL of water in a Teflon-lined steel autoclave and slowly adding 5 mL of solution **A** or **B** under stirring. The solution (**A** or **B**) was cooled in ice water to ca. 5°C before mixing. The temperature of the milky gel after mixing was 20–30°C. After heating the gel at a fixed temperature, it settled to a white powder. The crystalline material was washed with water, recovered using vacuum filtration and dried under ambient conditions.

The composition (molar ratios) of the reactants in the initially formed gels were approximately, (series **A**) ***n*** LiOH:1.0 $Zn(NO_3)_2$:1.0 H_3PO_4:ca. 160 H_2O and $C(PO_4^{3-}) \approx 0.30$ M or (series **B**) ***n*** LiOH:1.0 $Zn(NO_3)_2$:1.0 H_3PO_4:ca. 100 H_2O and $C(PO_4^{3-}) \approx 0.48$ M. The relative amount of lithium hydroxide, ***n***, was varied in the range, $1 < \boldsymbol{n} < 5$, $\boldsymbol{n} = n(\mathrm{Li})/n(PO_4)$, and the mixtures were placed at a fixed temperature in the range 20–240°C for 5–10 days.

Further series of experiments were performed using a similar method as described above in the system, ***n*** LiOH:***m*** $Zn(NO_3)_2$:1.0 H_3PO_4:ca. 100 H_2O, ($\boldsymbol{m} = n(\mathrm{Zn})/n(PO_4)$, $\boldsymbol{m} \neq 1$). A number of other experiments were performed using varying ratio of $LiOH/LiNO_3$ allowing independent variation of the relative amount of lithium ions, ***n***, and pH of the gel.

Hydrothermal syntheses experiments at temperatures above the critical temperature of water (374°C) were performed in a 2 mL sealed gold ampoule placed in a water-filled 7 mL steel pressure vessel allowing an external water pressure to be applied. Reactants were powder of α-$LiZnPO_4 \cdot H_2O$ suspended in water and added $LiNO_3$, LiCl and/or H_3PO_4. The used α-$LiZnPO_4 \cdot H_2O$ was prepared according to Ref. (3). Table 1 lists the initial composition of the reaction mixtures and experimental conditions for a few of the syntheses performed. Experiment no. 5 in Table 1 (denoted batch I) describes the synthesis of α-$Li_4Zn(PO_4)_2$ used for further structural investigation.

The syntheses were performed using the following commercial chemicals: $LiOH \cdot H_2O$ (Fluka, puriss p.a., > 99%), $LiNO_3$ (Merck, > 98%), LiCl (Merck, pro analysi, > 99%), H_3PO_4 (85%, Fluka, extra pure) and $Zn(NO_3)_2 \cdot 6H_2O$ (Fluka, purum p.a., > 99.0%).

TABLE 1
Hydrothermal Conversion of α-$LiZnPO_4 \cdot H_2O$ Suspended in Water[a]

	Initial composition								
Expt No.	Li	Zn	PO_4	H_2O	Products	pH	T (°C)	p (kbar)	t (h)
1	1.1	0.2	1	~17	α-$LiZnPO_4$	Acidic	580	2.13	24
2	4	1	1	~130	ε-$LiZnPO_4$	Acidic	380	2.07	76
3	2	0.5	1	~30	ε-$LiZnPO_4$	Acidic	400	2.07	76
4	1	1	1	~80	δ_I-$LiZnPO_4$ and α-$Li_4Zn(PO_4)_2$	Neutral	395	2.76	76
5	7	1	1	~120	α-$Li_4Zn(PO_4)_2$	Neutral	602	1.89	24

[a] H_3PO_4 was added in experiments 1–3, $LiNO_3$ was added in experiments 1, 2 and 5, and LiCl in experiment 3. The experiments were performed in Au ampoules.

2.2. Powder X-Ray Diffraction

Powder diffraction data for phase identification and refinement of unit cell parameters were obtained in transmission geometry using a Stoe diffractometer equipped with a curved Ge(111) monochromator (Cu$K\alpha_1$ radiation, $\lambda = 1.54060$ Å) and a linear position sensitive detector covering 6.3°. Room temperature data were collected from 5 to 88° in 2θ with counting time of 180–1200 s per step. The sample was mounted on foil and in a quartz capillary (0.5 mm) for RT and high-temperature data, respectively. The sample had α-Al_2O_3 as an internal standard and overlapping reflections are omitted. The program ALLHKL (25) was used to refine the unit cell parameters by full pattern profile fits. The refined monoclinic unit cell dimensions of α-$Li_4Zn(PO_4)_2$ were $a = 8.103(3)$ Å, $b = 10.260(5)$ Å, $c = 8.120(4)$ Å and $\beta = 104.9(1)°$, $V = 652.8(7)$ Å^3 (335 reflections were used in the refinement, $R_w = 0.061$). The indexed powder pattern of α-$Li_4Zn(PO_4)_2$ (25 reflections with $I/I_o > 1\%$ and $2\theta < 43°$, $M(25) = 10.7$) measured at RT is provided in Table 2.

A Stoe high-temperature furnace was mounted on the diffractometer to record powder patterns in situ in the temperature range 50–950°C. α-$Li_4Zn(PO_4)_2$ has a reversible phase transition to a high-temperature polymorph, β-$Li_4Zn(PO_4)_2$ at $T = 425$°C (22, 24). The powder pattern of the β-phase measured at $T = 900$°C was indexed using the DICVOL program (26) and a triclinic unit cell was suggested. Full pattern profile fits using the program ALLHKL (25) was performed for all powder patterns measured at elevated temperature in order to investigate the thermal expansion of the unit cell: space group $P\bar{1}$, $a = 5.173(3)$ Å, $b = 7.97(1)$ Å, $c = 9.92(1)$ Å, $\alpha = 80.9(1)$, $\beta = 126.8(1)$ and $\gamma = 106.0(1)°$, $V = 319.8(7)$ Å^3 and $Z = 2$ (138 reflections were used in the refinement, $R_w = 0.073$). The indexed powder pattern of β-$Li_4Zn(PO_4)_2$ (20 reflections with $I/I_o > 5\%$ and $2\theta < 55.3°$) measured at $T = 900$°C is provided in Table 3.

TABLE 2

Indexed Powder Pattern of α-$Li_4Zn(PO_4)_2$, Based on a Monoclinic Unit Cell: $a = 8.103(3)$ Å, $b = 10.260(5)$ Å, $c = 8.120(4)$ Å, and $\beta = 104.9(1)°$, $V = 652.8(7)$ Å^3 (25 Reflections with $I/I_0 > 1\%$ and $2\theta < 43°$, Cu$K\alpha_1$ Radiation, $\lambda = 1.54060$ Å)[a]

$2th_{obs}$	$2th_{calc}$	d_{obs}	d_{calc}	I_{obs}	h	k	l
11.34	11.41	7.797	7.750	21	0	0	1
14.27	14.34	6.202	6.174	42	0	1	1
	14.22		6.222		1	1	0
16.33	16.33	5.424	5.423	25	1	1	−1
20.78	20.82	4.271	4.264	21	0	2	1
	20.74		4.280		1	2	0
22.26	22.25	3.990	3.991	100	1	2	−1
22.60	22.60	3.931	3.932	63	2	0	−1
	22.65		3.923		2	0	0
22.94	22.93	3.874	3.875	50	0	0	2
24.29	24.24	3.661	3.669	34	2	1	−1
	24.28		3.662		2	1	0
24.44	24.43	3.639	3.640	3	1	1	−2
24.55	24.55	3.623	3.623	30	0	1	2
28.00	27.99	3.184	3.185	1	2	0	1
28.60	28.56	3.119	3.123	20	1	3	0
	28.63		3.115		2	2	−1
29.35	29.35	3.041	3.041	4	2	1	1
29.50	29.52	3.026	3.024	12	1	1	2
29.70	29.70	3.006	3.005	10	1	3	−1
31.95	31.95	2.799	2.799	19	1	3	1
33.01	33.01	2.711	2.711	41	2	2	−2
34.36	34.36	2.608	2.608	47	3	1	−1
34.75	34.83	2.579	2.574	35	2	3	−1
	34.74		2.580		1	1	−3
35.40	35.40	2.534	2.534	39	3	1	0
36.42	36.35	2.465	2.470	55	2	0	−3
37.00	37.04	2.428	2.425	7	0	4	1
	37.00		2.428		1	4	0
38.82	38.81	2.318	2.318	5	1	3	2
40.17	40.08	2.243	2.248	4	3	1	1
42.73	42.74	2.114	2.114	17	3	3	−1

[a] The X-ray data is measured at RT.

2.3. Single-Crystal X-Ray Diffraction

In house single-crystal diffraction data (sealed X-ray tube, Mo$K\alpha$) were too weak to allow structural analysis of α-$Li_4Zn(PO_4)_2$. Therefore, synchrotron X-ray diffraction data were measured at beamline X7B, NSLS, Brookhaven National Laboratory, USA (27), on a single crystal ($89 \times 35 \times 35\ \mu m^3$, see Table 1, no. 5). The wavelength was refined from a powder pattern of LaB_6 to, $\lambda = 0.9346(1)$ Å at $T = 25(2)$°C. Further experimental details are given in Table 4.

The data from NSLS showed some tendency towards orthorhombic symmetry (suggested space group $C222_1$, in agreement with Ref. (22), but the internal agreement of reflections improved by going to monoclinic symmetry with a cell whose a and c-axis are nearly equal and form the half diagonals of the orthorhombic cell. The space group suggested was $P2_1$ (in agreement with Ref. (23)). The heavier atoms could be found with this model, but the model could not be improved to give the light atoms. A dataset reindexed to fit the orthorhombic cell also gave the heaviest atoms, but would not solve any further. The idea now occurred that the crystal was indeed a twin thus giving rise to the extra symmetry. A model of a layer of the reciprocal lattice shows that superimposing the two monoclinic lattices, as illustrated in Fig. 1 can generate the apparent orthorhombic symmetry. If the two twins are equally strong, apparent perfect orthorhombic symmetry is obtained and would cause serious difficulties finding a structural model. In this case one twin was a bit stronger

TABLE 3

Powder Diffraction Data of β-$Li_4Zn(PO_4)_2$ Measured in Situ at $T = 900°C$, Indexed with a Triclinic Cell, $a = 5.173(3)$ Å, $b = 7.97(1)$ Å, $c = 9.92(1)$ Å, $\alpha = 80.9(1)°$, $\beta = 126.8(1)°$, and $\gamma = 106.0(1)°$, $V = 319.8(7)$ Å^3 (20 Reflections with $I/I_o > 5\%$ and $2\theta < 55.3°$, Cu$K\alpha_1$ Radiation, $\lambda = 1.54060$ Å)

$2\theta_{obs}$	$2\theta_{cal}$	d_{obs}	d_{calc}	I_{obs}	h	k	l
22.03	22.02	4.032	4.034	100	1	0	0
22.36	22.34	3.973	3.975	84	0	0	2
23.92	23.90	3.717	3.719	5	1	1	−1
25.70	25.68	3.464	3.466	5	0	2	1
27.27	27.20	3.268	3.277	8	1	1	0
31.68	31.68	2.822	2.822	49	1	1	−3
32.39	32.36	2.762	2.764	51	0	2	−2
33.81	33.80	2.649	2.650	31	0	0	3
34.51	34.50	2.597	2.597	53	1	2	−2
34.88	34.86	2.571	2.571	45	0	3	0
35.75	35.72	2.510	2.512	65	1	2	0
36.22	36.22	2.478	2.479	76	2	0	−2
36.90	36.88	2.434	2.435	19	2	0	−3
41.90	41.86	2.154	2.156	7	0	3	2
46.05	46.02	1.969	1.971	9	1	3	0
47.58	47.58	1.909	1.910	20	1	0	−5
48.95	48.96	1.859	1.859	16	1	3	−3
50.85	50.80	1.794	1.796	6	1	3	1
52.82	52.78	1.732	1.733	5	0	4	2
55.31	55.31	1.660	1.659	8	1	3	−4

TABLE 4

Experimental Conditions and Crystallographic Parameters for Single-Crystal Study of α-$Li_4Zn(PO_4)_2$ Using X-Ray Radiation Generated at the Synchrotron NSLS, Brookhaven National Laboratory at Beamline X7B Equipped with a MAR Area Detector

Crystal data	
$Li_4O_8P_2Zn$	Transparent
Dimensions	$35 \times 35 \times 89\ \mu m^3$
Crystal system	Monoclinic
Space group	$P2_1/a$ (No. 14)
Unit cell	$a = 8.096(2)$ Å
	$b = 10.242(2)$ Å
	$c = 8.106(2)$ Å
	$\beta = 104.73(3)°$
	$V = 650.1(2)$ Å^3
	$Z = 4$
	$M = 283.09$ g/mol
	$D_{calc} = 2.892$ g/cm^3
	$F_{ooo} = 544$
Data collection	
Measured reflections	1614
Independent reflections	968
$\theta_{min/max} = 3.4-31.1°$	
$T = 293(2)$ K	
$\lambda = 0.93547$ Å	
Refinement	
Full matrix on F^2	
Data, parameters	968, 67
Observed refl.	616 $F_o^2 > 3\sigma(F_o^2)$
Weighting scheme:	$w = (\sigma^2(F_o^2) + (0.091P)^2)^{-1}$
	$P = (F_o^2 + 2F_c^2)/3$
$R(F) = 0.042$	
$wR(F^2) = 0.068$	
$\Delta\rho_{min} = -1.6(3)$ eÅ^{-3}	
$\Delta\rho_{max} = 1.8(3)$ eÅ^{-3}	

than the other so that we would be comparing two spots: $\boldsymbol{I}(h,k,l,\text{twin1}) + \boldsymbol{I}(l,k,h,\text{twin2})$ on one side and $\boldsymbol{I}(l,k,h,\text{twin1}) + \boldsymbol{I}(h,k,l,\text{twin2})$ on the other side. The differences were clear and apparently random.

A set of reflections was constructed where the differences between $\boldsymbol{I}(h,k,l)$ and $\boldsymbol{I}(l,k,h)$ were made four times as big as in the real dataset preserving the sum of the two reflections. The structure solution, using the program SIR97 (28) now went perfectly (space group still $P2_1$) and all atoms were found. A look at the data showed that the $h0l$ reflections with h odd in the modified file were practically zero and the structure now also fitted $P2_1/a$. In fact the $(h,0,l)$ reflections with one odd index were the only reflections with only one twin contributing, and those with h and l both odd are actually absent. This peculiar absence rule would have been the only clue to the twinning in case of a 50/50 twin.

The structural model space group $P2_1$ initially refined against the modified dataset was now refined against the original data in space group $P2_1/a$ using a modified version of the least-squares program (29), based on the ORFLS program (30). This program allowed comparison of each reflection of the original dataset to the sum of $\boldsymbol{I}(h,k,l)$ and $\boldsymbol{I}(l,k,h)$ using separate scale factors and with the appropriate contributions to all derivatives. The scale factors correspond to a twin ratio of 59.5:40.5.

The structure refined to $R(F) = 0.042$ in space group $P2_1/a$, with no indication that a lower symmetry should be preferable. On the contrary the structure exhibits an approximate c-glide symmetry except that this would relate Zn to Li3 and leave Li4 with no counterpart. This together with the twinning means that the refinement is not very robust, and only Zn was allowed anisotropic displacement parameters. The twinning, on the other hand, is due to the local mirror plane through the phosphate groups parallel to the diagonal in the a,c-plane illustrated in Fig. 2 as an Ortep-style view. Further experimental details on the refinement are given in Table 4 along with atomic coordinates in Table 5. Figures 2 and 5 were drawn using the program Ortep (31) and the program Atoms (32) was used for preparation of the polyhedra drawings, Fig. 4.

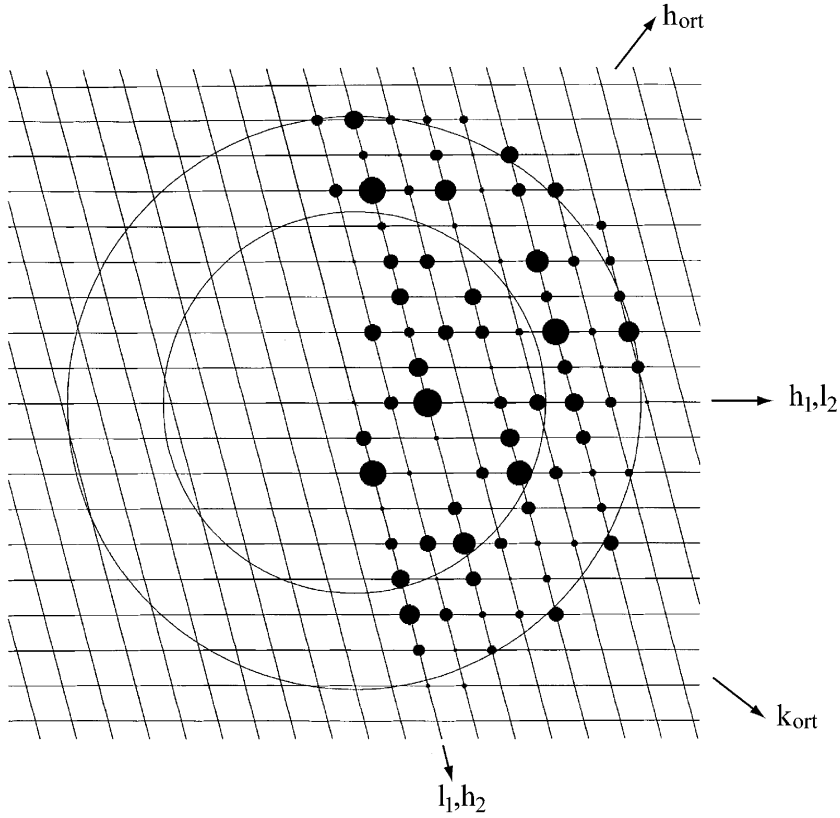

FIG. 1. Weighted reciprocal lattice (*h*0*l*) showing pseudo-orthorhombic symmetry.

3. RESULTS AND DISCUSSION

3.1. Hydrothermal Synthesis

The stability fields of the lithium zinc orthophosphates found in the system, LiOH:$Zn(NO_3)_2$:H_3PO_4:H_2O, are shown in Figs. 3A and 3B, displaying the range, $2.5 < \boldsymbol{n} < 4.5$ and $50 < T < 200$°C. Zeolite-type ABW α-$LiZnPO_4 \cdot H_2O$ (triangles) forms at low temperatures, $T <$ ca.120°C, in the range 2.5 to ca. 4.5 of $\boldsymbol{n}$ at relatively low phosphate concentrations, $C(PO_4^{3-}) \approx 0.30$ M (series **A**) but at $\boldsymbol{n} >$ ca. 3.1 at higher phosphate concentrations $C(PO_4^{3-}) \approx 0.48$ M (series **B**). The cristobalite-related material, δ_1-$LiZnPO_4$ (cross) (7, 10) forms at higher temperatures, $T >$ ca. 120°C in the same range, $\boldsymbol{n} >$ ca. 3. The dense phase α-$LiZnPO_4$ (circles) (11–13) forms at low pH, $\boldsymbol{n} <$ ca. 3.0 in series **A** and **B**, but only at $T >$ ca. 80°C in **A**. Further decreasing the amount of LiOH gives increasing amounts of Hopeite, $Zn_3(PO_4)_2 \cdot 4H_2O$. In all cases increasing amounts of β-Li_3PO_4 and ZnO were found at high concentration of lithium, at $\boldsymbol{n} >$ ca. 4. Experiments at 20°C gave similar results as those presented in Fig. 3 at $T = 70$°C. Furthermore, the phase stability fields at $T = 180$°C extend up to 240°C with the only change that a zinc phosphate mono hydrate, $Zn_3(PO_4)_2 \cdot H_2O$ (33), tends to form instead of Hopeite.

The hydrothermal stability fields of the zeolite-type ABW lithium zinc phosphates, α- and β-$LiZnPO_4 \cdot H_2O$ (7, 8), are remarkably different when $Zn(NO_3)_2 \cdot 6H_2O$ are substituted for $Zn(Ac)_2 \cdot 2H_2O$ in the synthesis. The β-phase was not observed when the nitrate was used as Zn source as illustrated in Fig. 3, in contrast, both the α- and β-phases could be prepared when zinc acetate was used. Furthermore, it was shown that α-$LiZnPO_4 \cdot H_2O$ can be converted to β (8).

Further experiments were performed in the system, $\boldsymbol{n}$ LiOH:$\boldsymbol{m}$ $Zn(NO_3)_2$:1.0 H_3PO_4:ca. 100 H_2O, in a search for novel materials or hydrothermal synthesis methods for other phases discovered by Torres-Trevino and West (22). Increasing the amount of Zn at low pH tends to give Hopeite, $Zn_3(PO_4)_2 \cdot 4H_2O$. Independent variation of the relative amount of substance of lithium ions, $\boldsymbol{n}$, and pH of the gel using varying ratio of $LiOH/LiNO_3$ suggest that pH is a more important structure-directing factor than $\boldsymbol{n}$.

In some cases metastable microporous materials can serve as precursors in the preparation of other new materials; this technique is named chimie douce (34). Table 1 shows materials prepared by conversion of zeolite type,

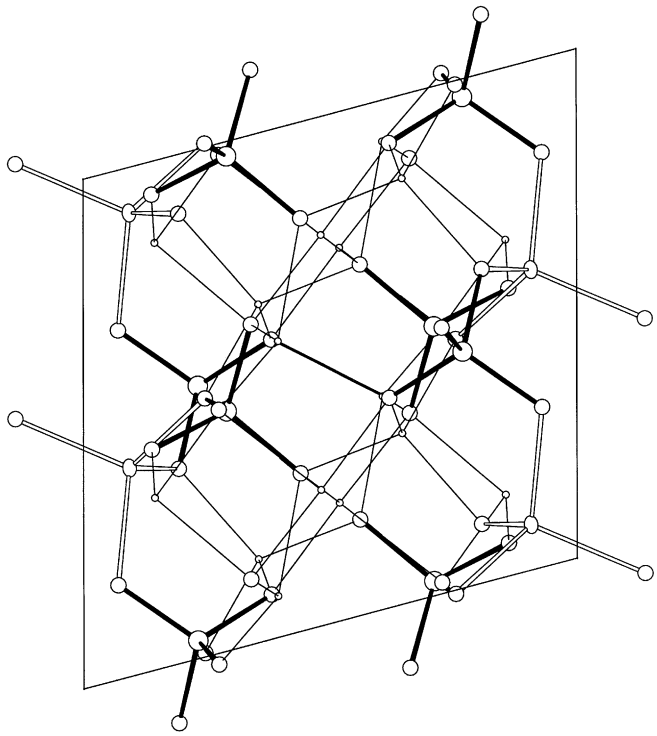

FIG. 2. The crystal structure of α-$Li_4Zn(PO_4)_2$ shown as an Ortep-style view of the *a*,*c*-projection. Zn ellipse and Zn–O bonds open, P and O circles and P–O bonds filled, lithium small circles and Li–O bonds shown as a single line.

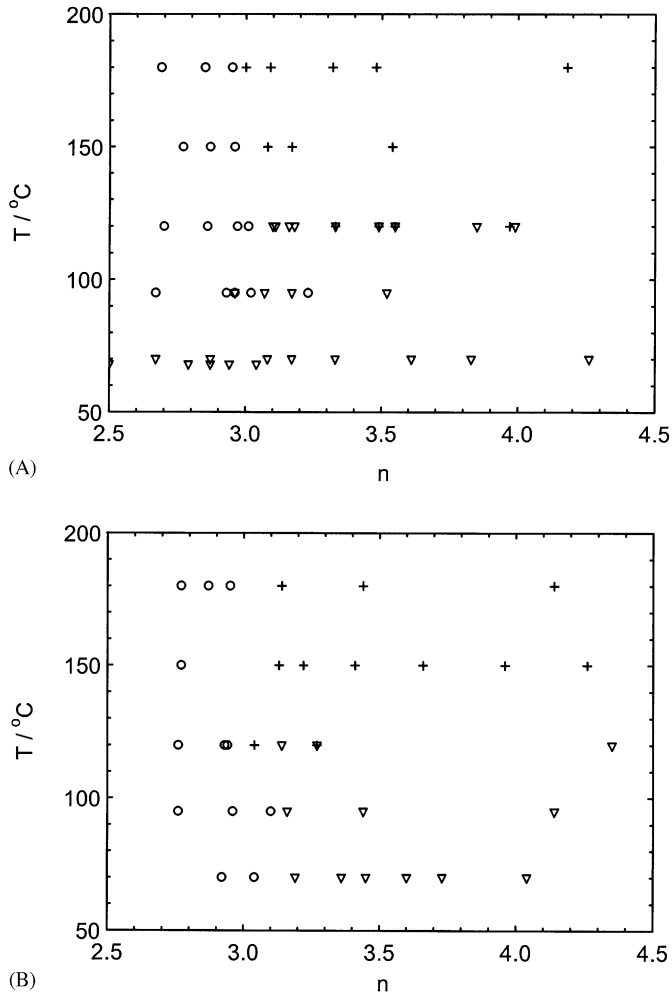

FIG. 3. The stability fields of lithium zinc orthophosphates found in the system, ***n*** LiOH:1.0 $Zn(NO_3)_2$:1.0 H_3PO_4:ca. 160 (**A**) or 100 (**B**) H_2O. Upper figure, series **A**, $C(PO_4^{3-}) \approx 0.30$ M and lower, series **B**, $C(PO_4^{3-}) \approx 0.48$ M. α-$LiZnPO_4 \cdot H_2O$ shown as triangles, δ_I-$LiZnPO_4$ as cross and α-$LiZnPO_4$ as circles.

α-$LiZnPO_4 \cdot H_2O$ using supercritical water as solvent ($T > 374°C$) Experiments 1–3 show that ε and α-$LiZnPO_4$ can be prepared in acidic solution using α-$LiZnPO_4 \cdot H_2O$ as precursor. In a neutral to slightly acidic solution, δ_I-$LiZnPO_4$ and α-$Li_4Zn(PO_4)_2$ can be prepared. The results presented in Table 1 correspond to the study of the system $LiOH:Zn(NO_3)_2:H_3PO_4:H_2O$ at higher temperature than illustrated in Fig. 3.

TABLE 5
Fractional Atomic Coordinates and Equivalent Isotropic Displacement Parameters of α-$Li_4Zn(PO_4)_2$

Atom	*X*	*Y*	*Z*	U_{eq}
Zn	−0.4101(3)	0.6566(2)	0.0907(3)	0.006(1)
P1	−0.4711(6)	0.4085(5)	0.2888(6)	0.004(3)
P2	−0.5343(6)	0.9078(5)	0.2301(6)	0.003(3)
O1	−0.625(2)	0.348(1)	0.344(2)	0.007(7)
O2	−0.317(1)	0.400(1)	0.442(2)	0.001(7)
O3	−0.443(2)	0.335(1)	0.133(2)	0.015(8)
O4	−0.506(2)	0.555(1)	0.242(2)	0.009(8)
O5	−0.587(2)	0.842(1)	0.385(2)	0.004(7)
O6	−0.684(2)	0.900(1)	0.067(2)	0.005(7)
O7	−0.387(2)	0.834(1)	0.191(2)	0.011(8)
O8	−0.482(2)	1.052(1)	0.274(2)	0.013(8)
Li1	−0.411(8)	0.826(6)	0.602(7)	0.063(14)
Li2	−0.655(6)	0.668(5)	0.358(6)	0.034(11)
Li3	−0.734(5)	0.929(4)	0.524(5)	0.023(8)
Li4	−0.646(5)	0.855(4)	0.862(5)	0.018(8)

3.2. Crystal Structure of α-$Li_4Zn(PO_4)_2$

Selected bond lengths and angles from the structural model of α-$Li_4Zn(PO_4)_2$ are given in Table 6. Zinc and phosphorus are coordinated to four oxygens each forming regular tetrahedra, whereas the LiO_4 tetrahedra are somewhat distorted. Four oxygens, O(3–6), are coordinated to three cations, Zn, P(1 or 2) and Li(1 or 2), whereas four oxygens, O(1, 2, 7 and 8), coordinate to four cations, P and three Li. Oxidation states, V_i, were calculated as a sum of

TABLE 6
Selected Bond Lengths (Å) and Bond Angles (deg) of α-$Li_4Zn(PO_4)_2$

Zn	O4	1.926(7)	O4	Zn	O5	104.3(3)
Zn	O5	1.943(7)	O4	Zn	O6	116.4(3)
Zn	O6	1.958(6)	O3	Zn	O4	111.6(3)
Zn	O3	1.969(7)	O5	Zn	O6	107.1(3)
Mean		1.949	O3	Zn	O5	109.1(3)
			O3	Zn	O6	108.0(3)
P1	O3	1.536(7)	O2	P1	O3	107.7(4)
P1	O2	1.540(7)	O1	P1	O3	110.3(4)
P1	O1	1.556(7)	O3	P1	O4	111.2(4)
P1	O4	1.561(7)	O1	P1	O2	111.0(3)
Mean		1.548	O2	P1	O4	107.9(4)
			O1	P1	O4	108.7(4)
P2	O7	1.515(7)	O6	P2	O7	109.1(4)
P2	O6	1.541(6)	O7	P2	O8	110.7(4)
P2	O8	1.541(7)	O5	P2	O7	109.9(4)
P2	O5	1.565(7)	O6	P2	O8	111.9(4)
Mean		1.541	O5	P2	O6	107.0(3)
			O5	P2	O8	108.0(4)
			O5	P2	O8	108.0(4)
Li1	O6	1.833(15)	O6	Li1	O8	126.9(8)
Li1	O8	1.978(15)	O1	Li1	O6	119.2(8)
Li1	O1	2.001(15)	O3	Li1	O6	108.8(7)
Li1	O3	2.111(15)	O1	Li1	O8	94.9(6)
Mean		1.981	O3	Li1	O8	101.3(7)
			O1	Li1	O3	102.1(7)
Li2	O2	1.881(14)	O2	Li2	O7	111.5(7)
Li2	O7	1.902(14)	O2	Li2	O5	109.0(7)
Li2	O5	1.914(15)	O2	Li2	O4	112.6(7)
Li2	O4	2.077(15)	O5	Li2	O7	107.0(7)
Mean		1.944	O4	Li2	O7	110.8(7)
			O4	Li2	O5	105.6(7)
Li3	O8	1.825(14)	O1	Li3	O8	125.1(7)
Li3	O1	1.991(14)	O7	Li3	O8	100.2(6)
Li3	O7	2.004(14)	O2	Li3	O8	117.3(7)
Li3	O2	2.086(14)	O1	Li3	O7	106.3(6)
Mean		1.977	O1	Li3	O2	101.3(6)
			O2	Li3	O7	104.7(6)
Li4	O2	1.962(19)	O1	Li4	O2	112.0(9)
Li4	O1	1.961(20)	O2	Li4	O7	111.3(9)
Li4	O7	2.002(20)	O2	Li4	O8	106.5(9)
Li4	O8	2.078(20)	O1	Li4	O7	132.7(10)
Mean		2.001	O1	Li4	O8	93.0(8)
			O7	Li4	O8	92.1(8)

bond valences, s, using the equation: $s = \exp[(r_o - r)/B]$, where r_o and B are empirical parameters and r is the bond length from the refined structural model given in Table 6 (35). The calculated oxidation states V_i, for the structural model are in agreement with the expected oxidation states, 4.82, 4.92, 2.06, 1.03, 1.12, 1.04, 0.95 for the cations P, Zn and Li, respectively.

The crystal structure of α-$Li_4Zn(PO_4)_2$ projected onto the *a*,*c*-plane is shown in Fig. 2. In this view of the structure, the cations form layers parallel to the long diagonal in the *a*,*c*-plane. Figure 4 visualizes the crystal structure of α-$Li_4Zn(PO_4)_2$ as polyhedra (P and Zn) and with Li shown as atoms. Fig. 4A shows the connectivity of tetrahedra in the *b*,*c*-plane revealing a layer-like connectivity of PO_4 and ZnO_4 interconnected by Li–O bonds. The (101) projection, Fig. 4B, reveals four-rings and apparent eight rings of PO_4 and ZnO_4 tetrahedra. The *a*,*b*-projection, Fig. 4C, shows that the four-rings of tetrahedra are placed at the corners and the center of the unit cell and that chains of tetrahedra are running in the direction of the *a*-axis.

The material, α-$Li_4Zn(PO_4)_2$, was initially structurally investigated by Belov *et al*. (23), who presented a structural model with twice as many atomic positions (space group $P2_1$) as found in this study (see Table 5). It is not clear whether this crystal was a twin as well. Another sample of α-$Li_4Zn(PO_4)_2$ also prepared by solid-state reaction was assigned an orthorhombic unit cell and space group $C222_1$ from powder diffraction data and Weissenberg photograph by Torres-Trevino and West (22). In this study, α-$Li_4Zn(PO_4)_2$ was prepared by hydrothermal methods and

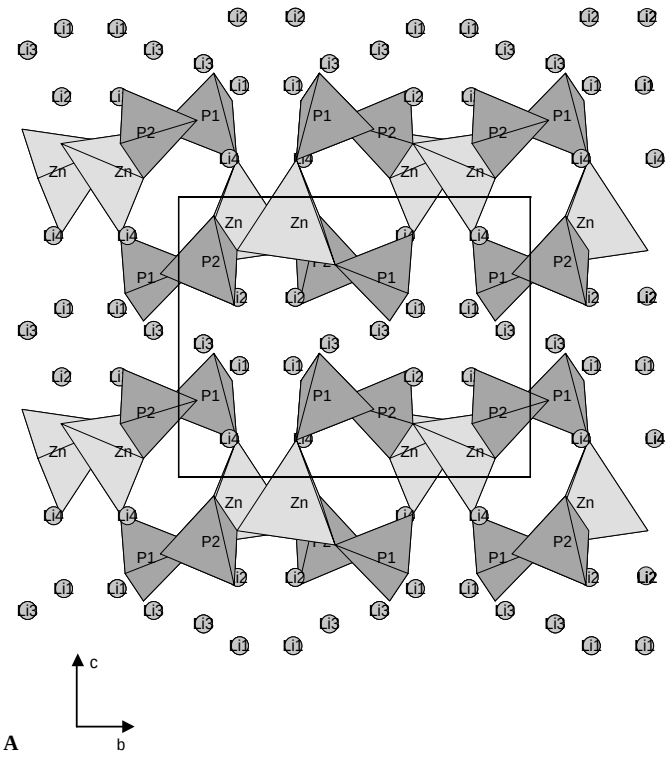

FIG. 4. The crystal structure α-$Li_4Zn(PO_4)_2$ with PO_4 and ZnO_4 shown as tetrahedra (dark and light, respectively) and Li atoms shown as circles. **A**, the *b*,*c*-projection. **B**, the (1 0 1) projection and **C**, the *a*,*b*-projection.

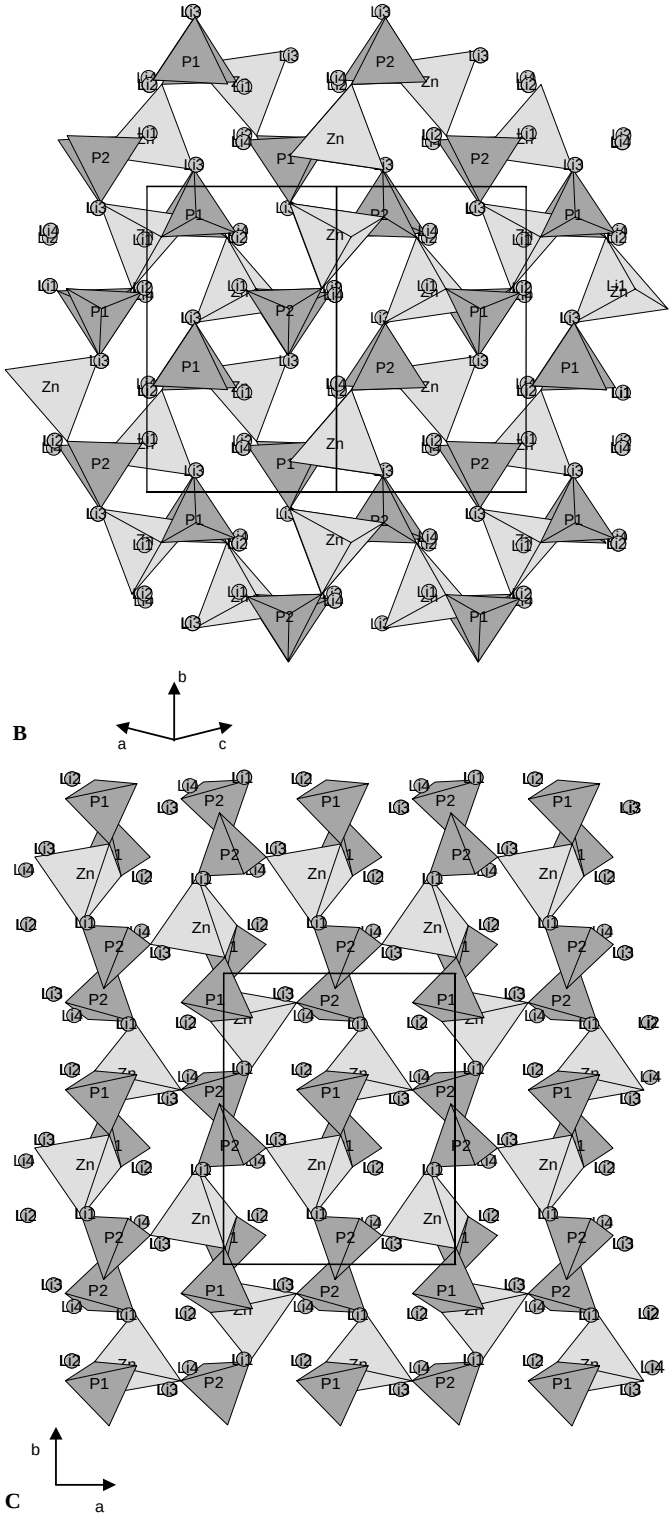

FIG. 4—*Continued*

the structural investigation was performed on a small crystal using high flux synchrotron X-ray radiation. It turns out that the structure of α-$Li_4Zn(PO_4)_2$ is related to the structure of γ-Li_3PO_4 (36) as illustrated in Fig. 5, showing an ortep view along a diagonal in the *a*,*c*-plane. The atomic positions of P and O in the two structures are similar but some Li vacancies are introduced by the virtual substitution of $Li^+ \rightarrow 1/2Zn^{2+}$ when the structure of γ-Li_3PO_4 is transformed to α-$Li_4Zn(PO_4)_2$. Substitution of $2Li^+ \rightarrow Zn^{2+}$ in the structure of γ-Li_3PO_4 (leaving the Li(1) position empty) gives the crystal structure of δ_I-$LiZnPO_4$, which is described as a cristobalite-related phase (10).

TABLE 7

Linear Thermal Expansion Coefficients of Unit Cell Parameters for α- and β-$Li_4Zn(PO_4)_2$ Calculated from in Situ Powder Diffraction Data

Phase	T (°C)	α_a ($10^{-5}\,K^{-1}$)	α_b ($10^{-5}\,K^{-1}$)	α_c ($10^{-5}\,K^{-1}$)	α_{vol}
α	50–400	0.86	0.20	2.5	3.5
β	450–900	1.8	1.3	2.0	8.5

3.3. *The High-Temperature Polymorph, β-$Li_4Zn(PO_4)_2$*

The measured in situ powder diffraction patterns of $Li_4Zn(PO_4)_2$ clearly show a phase transition from α to β

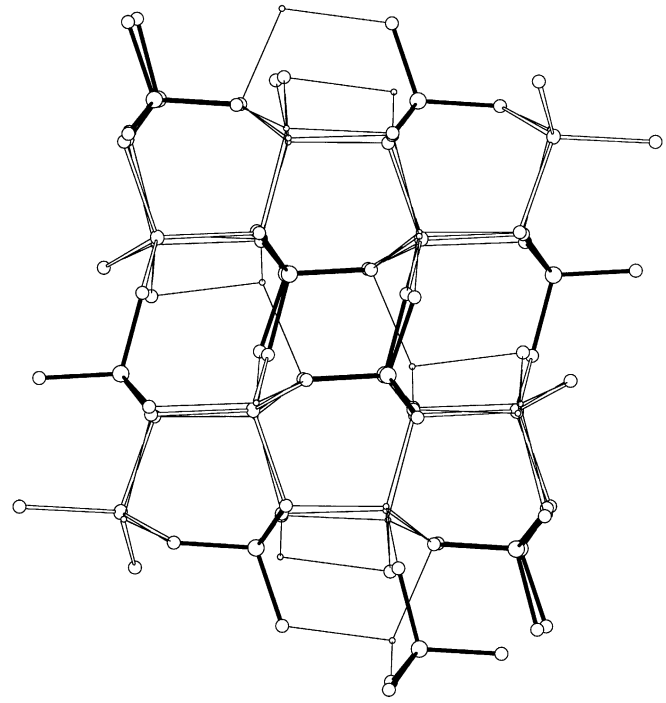

FIG. 5. The crystal structure of α-$Li_4Zn(PO_4)_2$ shown as an Ortep-style view of a projection spanned by a diagonal in the *a*,*c*-plane and the *b*-axis. Zn–O open bonds, filled P–O bonds and lithium shown as small circles.

between 400°C and 450°C as illustrated in Fig. 6. Torres-Trevino and West reported a reversible phase transition at $T = 425$°C (22, 24). Some reflections at low Bragg angle (2θ) are disappearing during the phase transition suggesting a reduced cell volume for the β-phase. Most of the reflections of the pattern recorded at 450°C can be indexed on a monoclinic cell with: $a/2, b, c, \beta$, using the unit cell parameters refined with X-ray data measured at 400°C. However, a triclinic cell gave a better full pattern fit in the temperature range 450–900°C (see Table 3). This cell has approximately half the cell volume of the α phase unit cell. An orthorhombic cell for β-$Li_4Zn(PO_4)_2$ was suggested based on RT data measured on a phase of $Li_4Zn(PO_4)_2$ with approximately 10% Si substituted for P (22), but this cell did not correspond satisfactorily to the in situ data measured in this work. Furthermore, it was suggested that this phase transition could be characterized as an order–disorder transition resembling the $\beta \rightarrow \gamma$ in Li_3PO_4 (22).

The thermal expansion of the unit cell of α- and β-$Li_4Zn(PO_4)_2$ is visualized in Fig. 7 and linear thermal expansion coefficients are extracted from this data and given in Table 7. The linear thermal expansion coefficients were calculated using the equation: $\alpha_L = (1/L_o)(\Delta L/\Delta T)$ where L denotes a unit cell axis or volume and L_o is the extrapolated value at $T = 0$°C. The linear thermal expansion coefficients for the unit cell volume of α- and β-$Li_4Zn(PO_4)_2$ is 3.5×10^{-5} and $8.5 \times 10^{-5}\,K^{-1}$, respectively, compared to values of 2.9×10^{-5} and $4.1 \times 10^{-5}\,K^{-1}$ found for the phenacite-related material α-$LiZnAsO_4$ in a similar temperature range (16).

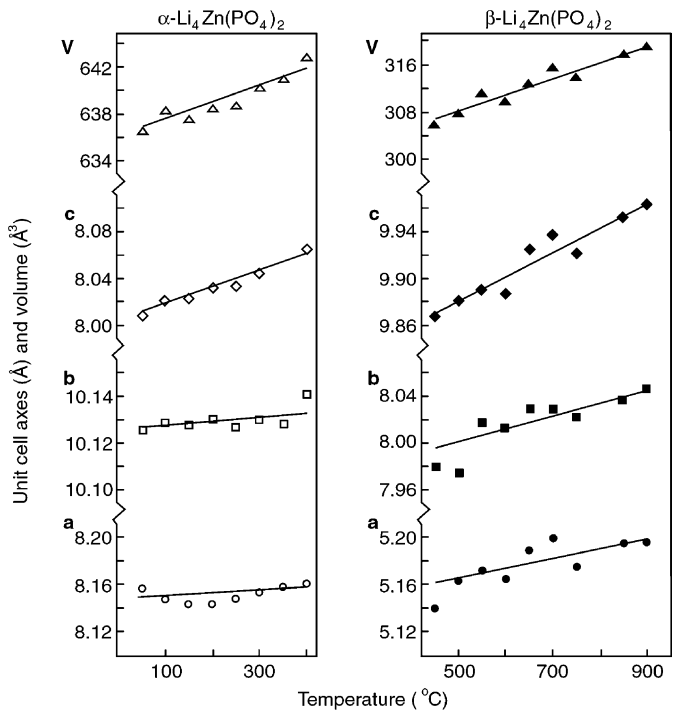

FIG. 7. Thermal expansion of α and β-$Li_4Zn(PO_4)_2$ illustrated by the unit cell axes and volume as a function of temperature in the range, $50°C < T < 900°C$.

3.4. Structure Comparison with Related Materials

The twin formation observed for α-$Li_4Zn(PO_4)_2$ can possibly be related to the phase transition at 425°C as the synthesis was performed at 602°C using supercritical water as solvent. A minor degree of disorder can, in principle, occur in lithium zinc phosphates because of the similarity in coordination radii of the Li and Zn ions. The mean bonds lengths ⟨Li–O⟩ and ⟨Zn–O⟩ are, 1.968 and 1.958 Å, respectively, calculated using the data for ε-, α-, CR1- and δ_I-$LiZnPO_4$ (7, 9–11, 14) (the mean bond length ⟨P–O⟩ is 1.539 Å for these compounds). Li/Zn disorder has been described in both silicates and germanates, e.g., $Li_{3.4}Si_{0.7}S_{0.3}O_4$, $Zn(Zn_{0.1}Li_{0.6}Si_{0.3})SiO_4$ and $Li_3Zn_{0.5}GeO_4$, prepared by solid-state reaction at high temperatures, 700–1000°C (37–40). Slight disorder was also proposed for δ_I-$LiZnPO_4$ prepared by hydrothermal synthesis and investigated using synchrotron X-ray powder diffraction (10). Table 8 summarizes the results from this investigation and provide an overview of other known phases of lithium zinc orthophosphates.

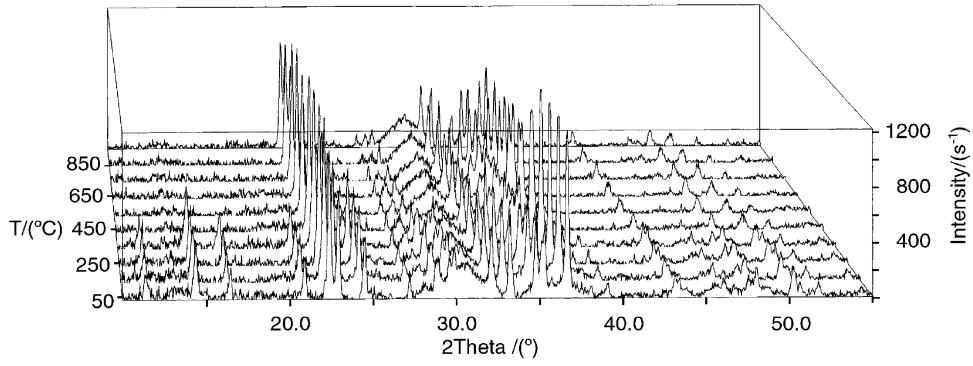

FIG. 6. Powder X-ray diffraction diagrams of the α- to β-$Li_4Zn(PO_4)_2$ phase transition measured in situ in the temperature range $20°C < T < 900°C$.

TABLE 8
Crystal Data of Some Lithium Zinc Orthophosphates Prepared by Hydrothermal or Solid State Synthesis

Compound	Space group	a (Å)	b (Å)	c (Å)	$\alpha/\beta/\gamma$ (deg)	Ref.
Hydrothermal synthesis						
α-$Li_4Zn(PO_4)_2$	$P2_1/a$	8.096	10.242	8.106	90/104.7/90	This work
β-$Li_4Zn(PO_4)_2$	P-1	5.173	7.97	9.92	80.9/126.8/106.0	This work
ε-$LiZnPO_4$	$R3$	13.628	13.628	9.9096	90/90/120	9
δ_I-$LiZnPO_4$	$Pna2_1$	10.019	4.966	6.675	90/90/90	7, 10
CR1-$LiZnPO_4$	Cc	17.2962	9.7753	16.1989	90/98.953/90	14
α-$LiZnPO_4 \cdot H_2O$	$Pna2_1$	10.575	8.076	4.994	90/90/90	7
β-$LiZnPO_4 \cdot H_2O$	$P2_1ab$	10.030	16.553	5.012	90/90/90	8
Solid-state reaction						
α-$LiZnPO_4$	Cc	17.250	9.767	17.106	90/110.9/90	11

4. CONCLUSION

Hydrothermal synthesis can act as an important alternative to solid-state reactions capable of providing high-quality material allowing structural investigation. Furthermore, the use of high flux and well-collimated X-ray beams from a synchrotron source can be utilized to explore challenging materials as twinned α-$Li_4Zn(PO_4)_2$. The twinning of α is possibly related to a phase transition at 425°C as the material was prepared at 602°C using supercritical water as solvent. A unit cell for the high-temperature polymorph β-$Li_4Zn(PO_4)_2$ is proposed along with an investigation of the thermal expansion.

ACKNOWLEDGMENTS

The Danish Natural Science Research Council under the program *DanSync* is gratefully acknowledged for financial support. Carlsberg Fondet is acknowledged for the high-temperature furnace used on the Stoe diffractometer. The research carried out at the National Synchrotron Light Source (NSLS) at Brookhaven National Laboratory is supported under contract DEAC 02-98CH10886 with the US Department of Energy by its Division of Chemical Science, Office of Basic Energy Science.

REFERENCES

1. P. Feng, X. Bu, and G. D. Stucky, *Nature (London)* **388,** 735 (1997).
2. X. Bu, P. Feng, and G. D. Stucky, *Science* **278,** 2080 (1997).
3. T. E. Gier and G. D. Stucky, *Nature (London)* **349,** 508 (1991).
4. V. Soghomonian, Q. Chen, R. C. Haushalter, J. Zubieta, and C. J. O'Connor, *Science* **259,** 1596 (1993).
5. Q. Huo, D. I. Margolese, U. Ciesla, P. Feng, T. E. Gier, P. Sieger, R. Leon, P. M. Petroff, F. Schüth, and G. D. Stucky, *Nature (London)* **368,** 317 (1994).
6. S. R. S. Prabaharan, M. S. Michael, S. Radhakrishna, and C. Julien, *J. Mater. Chem.* **7,** 1791 (1997).
7. W. T. A. Harrison, T. E. Gier, J. M. Nicol, and G. D. Stucky, *J. Solid State Chem.* **114,** 249 (1995).
8. T. R. Jensen, *J. Chem. Soc. Dalton Trans.* 2261 (1998).
9. X. Bu, T. E. Gier, and G. D. Stucky, *Acta Crystallogr. Sect. C* **52,** 1601 (1996).
10. T. R. Jensen, P. Norby, P. C. Stein, and A. M. T. Bell, *J. Solid State Chem.* **117,** 39 (1995).
11. L. Elammari, and B. Elouadi, *Acta Crystallogr. Sect. C* **45,** 1864 (1989).
12. G. Torres-Trevino and A. R. West, *J. Mater. Sci. Lett.* **4,** 1138 (1985).
13. A. Elfakir, J.-P. Souron, F. Robert, and M. Quarton, *C. R. Acad. Sci. Paris* **309,** 199 (1989).
14. X. Bu, T. E. Gier, and G. D. Stucky, *J. Solid State Chem.* **138,** 126 (1998).
15. A. Durif, *Bull. Soc. Franc. Minér. Crist.* **84,** 322 (1961).
16. T. R. Jensen, P. Norby, J. C. Hanson, E. M. Skou, and P. C. Stein, *J. Mater. Chem.* **8,** 969 (1998).
17. T. R. Jensen, P. Norby, and A. Nørlund Christensen, *Micropor. Mesopor. Mater.* **26,** 77 (1998).
18. W. T. A. Harrison, T. E. Gier, G. D. Stucky, R. W. Broach, and R. A. Bedard, *Chem. Mater.* **8,** 1145 (1996).
19. W. T. A. Harrison, T. M. Nenoff, T. E. Gier, and G. D. Stucky, *Inorg. Chem.* **32,** 2437 (1993).
20. T. R. Jensen, R. G. Hazell, T. Vosegaard, and H. J. Jakobsen, *Inorg. Chem.* **39,** 2026 (2000).
21. T. R. Jensen, and R. G. Hazell, *J. Chem. Soc. Dalton Trans.* **16,** 2831 (2000).
22. G. Torres-Trevino, and A. R. West, *J. Solid State Chem.* **61,** 56 (1986).
23. P. A. Sandomirskii, M. A. Simonov, and I. V. Belov, *Dokl. Akad. Nauk. SSSR* **228,** 344 (1976).
24. G. Torres-Trevino, and A. R. West, *J. Solid State Chem.* **71,** 381 (1987).
25. G. S. Pawley, *J. Appl. Crystallogr.* **14,** 357 (1981).
26. A. Boultif, and D. Louer, *J. Appl. Crystallogr.* **24,** 987 (1991).
27. J. B. Hastings, P. Suortti, W. Thomlinson, A. Kvick, and T. F. Koetzle, *Nucl. Instrum. Methods* **208,** 55 (1983).
28. A. Altomare, M. C. Burla, M. Camalli, G. L. Cascarano, C. Giacovazzo, A. Guagliardi, A. G. G. Moliterni, and G. Polidori, R. Spagna, *J. Appl. Crystallogr.* **32,** 115 (1999).
29. A. Hazell, KRYSTAL, "An Integrated System of Crystallographic Programs." University of Aarhus, Denmark, 1995.

30. W.T. Busing, K.O. Martin, and H.A. Levy, "ORFLS." Report ORNL-TM-305, Oak Ridge National Laboratory, Tennessee, USA, 1962.
31. M. N. Burnett, and C. K. Johnson, "ORTEP-III." Report ORNL-6895, Oak Ridge National Laboratory, Tennessee, USA, 1996.
32. E. Dowty, "Program ATOMS version 5.0." Shape Software, 521 Hidden Valley Road, Kingsport, TN 37663, USA, 1997.
33. A. Riou, Y. Cudennec, and Y. Gerault, *Rev. Chimie Miner.* **23,** 810 (1986).
34. J. Gopalakrishnan, *Chem. Mater.* **7,** 1265 (1995).
35. I. D. Brown, and D. Altermatt, *Acta Crystallogr. Sect. B* **41,** 244 (1985).
36. J. von Zeman, *Acta Crystollogr.* **13,** 863 (1960).
37. S. C. Yu, D. K. Smith, and S. B. Austerman, *Am. Mineral.* **63,** 1241 (1978).
38. A. N. Fitch, B. E. F. Fender, and J. Talbot, *J. Solid State Chem.* **55,** 14 (1984).
39. E. Plattner, and H. Völlenkle, *Monatsh Chem.* **110,** 693 (1979).
40. W. H. Baur, *Inorg. Nucl. Chem. Lett.* **16,** 525 (1980).